JOURNAL OF
EMERGING INVESTIGATORS

Article

A 3D printed triboelectric nanogenerator for bridge vibration energy harvesting and sensing

Vedant Walavalkar[1], Asrar Rafiq Bhat[2]
[1]Fravashi International Academy, Nashik, Maharashtra, India
[2] Metallurgical Engineering and Materials Science Department, IIT Bombay, Mumbai, Maharashtra, India

SUMMARY
Adopting renewable energy technologies is vital for a sustainable future. Triboelectric nanogenerators (TENGs) offer an innovative way to harvest ambient vibrational energy from sources like human motion, machinery, and structures. This enables practical applications such as self-powered sensors for structural health monitoring. One of the key challenges in practical TENG deployment is the fabrication of triboelectric layers with optimized surface and structural features that can enhance charge generation under such conditions. To address this, we used fused deposition modelling (FDM)-based 3D printing for the fabrication of TENG components due to its advantages in tailoring surface characteristics through parameter control. We hypothesized that optimizing specific 3D printing parameters, namely the infill pattern and layer height, would enhance the energy output of TENGs. To explore this, we designed and developed a 3D printed TENG-based prototype capable of harvesting energy from bridge vibrations and tested commonly available materials. The optimization process involved modifying critical parameters such as infill pattern and triboelectric layer height or thickness to achieve maximum performance. Results indicated that a combination of thermoplastic polyurethane/polyethylene terephthalate material, a tri-hexagonal infill pattern, and a layer height of 0.4 mm yielded the highest voltage output. This combination generated 11 V under a tapping frequency of approximately 3 Hz, demonstrating its suitability for bridge vibration energy harvesting by powering light-emitting diodes and charging a capacitor. This study demonstrates the potential of optimized 3D printing parameters in enhancing TENG performance, paving the way for efficient and scalable energy harvesting systems for real-world applications.

INTRODUCTION
A triboelectric nanogenerator (TENG) is an energy harvesting device that converts mechanical energy into electricity using the triboelectric effect. This effect involves static charge generation when two dissimilar materials repeatedly come into contact and separate. TENGs are innovative devices that turn everyday movements like walking or jogging into electrical energy by contact electrification and electrostatic induction (1). They play a crucial role in powering small gadgets and sensors, particularly in wearables, wireless pressure sensors, motion-activated light emitting diodes (LEDs), electronic wristbands, and environmental monitoring devices, offering a green, cost-effective energy source (2). As this field grows, TENGs are increasingly seen as a key component in the development of sustainable energy solutions, capable of harvesting ambient mechanical energy from daily activities. Emerging applications include blue energy harvesting from ocean waves, implantable biomedical devices, smart agriculture systems, and energy-scavenging pavements, where mechanical motion is abundant and traditional power sources are either limited or environmentally burdensome (3).

TENGs operate in different modes to generate electricity from mechanical energy (4). The most common, is the contact-separation mode, wherein two materials with different electron affinities repeatedly come into contact and separate **(Figure 1a)**. The initial contact causes contact electrification, and the subsequent separation induces electron flow via electrostatic induction (5). This mode is well-suited for applications involving repetitive motions, such as mechanical switches (6). Another is the lateral sliding mode, in which two triboelectric materials remain in contact while one slides over the other **(Figure 1b)**. This continuous relative motion generates a dynamic charge imbalance across the surface due to ongoing displacement, driving electron flow through the external circuit (7). Unlike contact-separation mode, which relies on vertical motion, sliding mode is effective in harvesting energy from horizontal or rotational movements (8). In lateral sliding mode, both triboelectric layers remain in physical contact, and electrodes are attached to each layer, allowing charge transfer through direct interface displacement (9). Each mode offers unique benefits and applications, making TENGs versatile for different energy-harvesting needs (10).

Bridges represent an especially compelling real-world application for TENG-based energy harvesting due to their constant exposure to mechanical stimuli such as wind, vehicular motion, and foot traffic. These large-scale structures experience both subtle and dynamic vibrations across multiple directions, offering ideal conditions for capturing ambient mechanical energy. Moreover, as critical infrastructure, bridges increasingly require continuous monitoring to ensure structural integrity and safety. Integrating TENGs into bridges enables not only self-powered sensing of vibrations and deformations but also supports the development of sustainable, maintenance-free systems for structural health monitoring. Their complex vibrational behaviour makes bridges an excellent model system for exploring the effectiveness of different TENG designs, materials, and operational modes in realistic, multidirectional environments.

One major issue is the difficulty in customizing TENGs to fit the specific vibrational patterns of large structures like bridges (11). Traditional manufacturing methods often fall short in creating designs that are tailored to these unique needs,

https://doi.org/10.59720/25-003

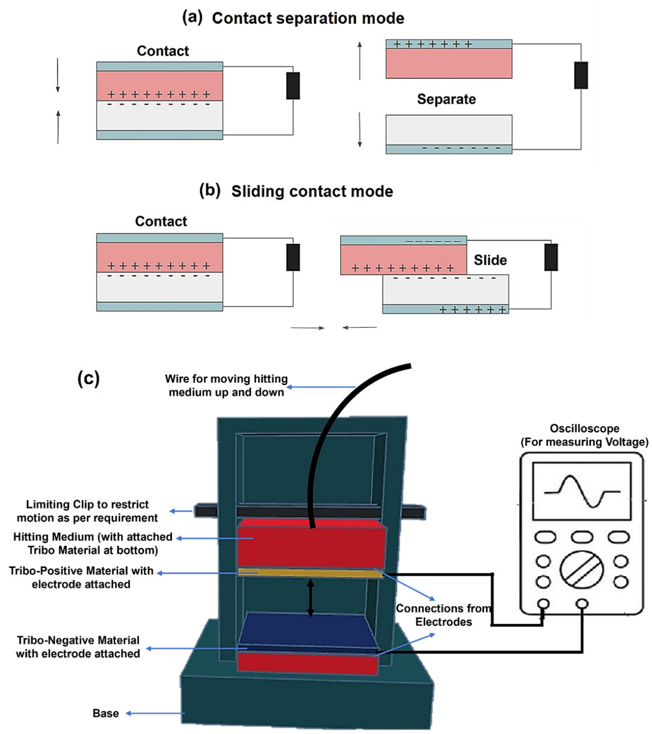

Figure 1: Operational modes of a triboelectric nanogenerator (TENG) and the custom testing setup used for systematic parameter optimization. (a) Contact-separation mode. The cycle begins with the contact of two dielectric materials with opposing triboelectric polarities (tribo-positive and tribo-negative), leading to static charge generation through contact electrification. Upon separation, a potential difference is created due to the charge imbalance, driving electrons through the external circuit via electrostatic induction resulting in electricity generation. (b) Sliding mode. A continuous charge imbalance is sustained by the relative lateral sliding motion between the two triboelectric materials. This displacement dynamically changes the overlapping contact area, inducing a continuous alternating current in the external circuit. (c) Cross sectional view of a testing tower. Inside the testing tower there is a hitting medium that can be moved up and down using a wire (to induce contact separation motion). The testing tower has grooves at both sides after every 2 cm from top to bottom. The limiting clip can be inserted into the groove to restrict motion of the hitting medium when it is moved up and down using a wire. At the bottom of the hitting medium and the base of testing tower triboelectric materials were attached. The triboelectric materials have electrodes attached at the back side that are in turn connected to wires. The tribo-negative layer was attached to the hitting medium, and the tribo-positive layer was fixed to the base, with a copper electrode connected to the back of each layer. The wires were connected to oscilloscope (shown on right side) for measuring the output voltage when contact and separation motions are given.

leading to less efficient energy capture (12). Additionally, the sensitivity of TENGs is crucial as it plays an important role for efficient energy harvesting as well as sensing the smallest vibrations caused by traffic or natural forces (13). Many current designs struggle with accurately capturing these subtle movements (14). The complex process of combining these components often leads to inefficiencies and reliability issues as well. Finally, scaling up the production of TENGs for real-world applications remains a significant hurdle, with cost and practicality being major barriers (15).

3D printing offers significant advantages in customizing and optimizing TENGs to enhance energy harvesting efficiency from bridge vibrations through rapid prototyping, design flexibility, and efficient material use (16). It enables the creation of complex and customized geometries that enhance triboelectric performance, which are difficult to achieve with traditional methods like casting or layer assembly. However, its adoption remains limited due to challenges in printing suitable triboelectric materials and concerns over resolution and mechanical durability (17). We propose a 3D-printed TENG specifically for harvesting energy from vibrations caused by wind and moving traffic on bridges. Given that bridge vibrations are complex and multi-directional, we employed a hybrid sliding and contact-separation mode TENG. This design is critical for capturing different vibrational components: the sliding mode efficiently harvests energy from the vertical motion of the internal slider against the casing, while the contact-separation mode activates during lateral displacements, where the slider makes and breaks contact with the sides of the enclosure. By combining these two mechanisms, the TENG can effectively harvest energy from the diverse and unpredictable motions characteristic of bridge vibrations, making it a robust and highly suitable solution for this application.

We hypothesized that optimizing specific 3D printing parameters, namely the infill pattern and layer height, would enhance the energy output of TENGs (18). Infill patterns influence surface roughness, which increases the effective contact area, thereby enhancing charge generation. For layer height, a balance must be achieved between sensitivity and output voltage as reducing it enhances sensitivity by lowering the force required for voltage generation, while increasing it maximizes the output. Since bridge vibrations can range from intense to very subtle, sensitivity becomes just as important as output voltage. A highly sensitive TENG is essential to effectively detect low-magnitude vibrations, making responsiveness a critical design criterion alongside voltage generation.

In summary, the results of this study strongly support our initial hypothesis that optimizing 3D printing parameters would enhance TENG performance. We confirmed that the infill pattern and layer height are critical factors, with the tri-hexagonal pattern and a 0.4 mm layer height identified as the optimal combination. This configuration collectively achieved a peak voltage output of up to 11.3 V, a significant enhancement over other tested parameters. These design improvements substantiate the potential of optimized, 3D-printed TENGs for developing scalable, cost-effective solutions for powering low-energy electronics, particularly in applications such as structural health monitoring.

RESULTS

The triboelectric performance of different material pairs was evaluated using a custom-built testing setup **(Figure 1c)**, with detailed methodology provided in the Materials and Methods section.

Material selection and optimization

Material selection is a crucial step in enhancing the

https://doi.org/10.59720/25-003

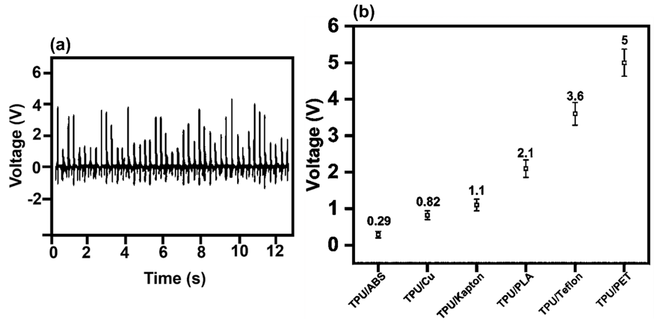

Figure 2. Triboelectric performance evaluation of different material pairs. (a) A representative oscilloscope waveform showing the output voltage from the optimal material pair, thermoplastic polyurethane (TPU) and polyethylene terephthalate (PET). The signal shows a peak-to-peak voltage of approximately 5 V. (b) Comparison of mean peak-to-peak voltage output for six different tribo-negative materials paired with a consistent TPU (tribo-positive) layer. The tested pairs were TPU/Acrylonitrile Butadiene Styrene (ABS), TPU/Copper (Cu), TPU/Kapton, TPU/Polylactic Acid (PLA), TPU/Teflon, and TPU/PET. The voltage for each pair was determined by averaging ten maximum peak-to-peak readings per sample. The data presented are the mean values from three independently tested samples (n=3). Error bars represent the standard deviation. The TPU/PET pair yielded a significantly higher output (~5 V) compared to all other combinations, with the TPU/ABS pair performing the lowest (~0.3 V).

triboelectric performance of TENGs (19). To optimize the triboelectric performance of our TENG prototype, we first sought to identify the most effective pair of materials. We tested a series of common tribo-negative materials against a consistent tribo-positive layer of thermoplastic polyurethane (TPU), which was selected for its flexibility, availability, and ease of 3D printing. The tested tribo-negative materials included acrylonitrile butadiene styrene (ABS), kapton, copper, polylactic acid (PLA), teflon, and polyethylene terephthalate (PET).

Our results indicate that the TPU/PET combination performed the best, generating a peak-to-peak voltage of approximately 5 V with a standard deviation of 0.09 V **(Figure 2a)**. This output was notably higher than the other combinations tested, with TPU/PET delivering approximately 16.67 times the voltage of the TPU/ABS combination, which performed the lowest among all pairs **(Figure 2b)**.

Effect of infill pattern

Following the material selection, we investigated the effects of various infill patterns on the triboelectric performance of 3D-printed TPU with the same testing setup. Infill refers to the internal structure or pattern used to fill the inside of a printed object. Infill patterns play a critical role in the triboelectric output, as they influence both the structural integrity and the frictional interactions between triboelectric surfaces (20). To maximize friction and improve the efficiency of energy conversion, we evaluated six distinct infill patterns newly incorporated in additive manufacturing: line, concentric, grid, cubic, octet, and tri-hexagon **(Figure 3a)**.

Our results demonstrated variability in voltage output across different patterns. The tri-hexagonal pattern consistently produced the highest voltage, achieving a mean peak-to-peak voltage output of approximately 11.3 V with a standard deviation of 0.56 V, which is more than double that of the line pattern **(Figure 3a-b)**. In contrast, the line infill pattern generated the lowest output, yielding a mean peak-to-peak voltage of 5.1 V with a standard deviation of 0.12 V **(Figure 3b)**.

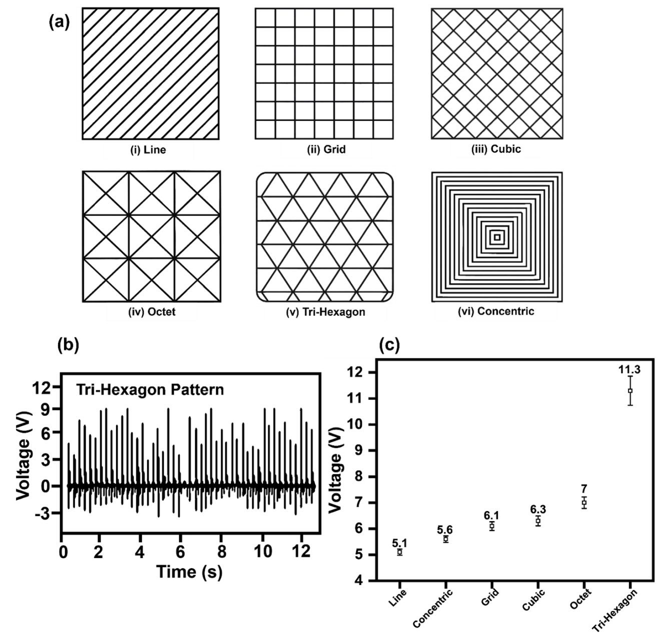

Figure 3. Optimization of triboelectric output through 3D printing infill patterns. (a) Schematic illustrations of the six distinct infill patterns tested for the thermoplastic polyurethane (TPU): (i) Line, (ii) Grid, (iii) Cubic, (iv) Octet, (v) Tri-Hexagon and (vi) Concentric. (b) A representative oscilloscope waveform of output voltage generated by the optimal tri-hexagon patterned TPU paired with a polyethylene terephthalate (PET). The signal corresponds to the highest recorded mean peak-to-peak voltage of approximately 11.3 V. (c) A graph comparing the mean peak-to-peak voltage output for TPU layers printed with the different infill patterns (Line, Grid, Cubic, Octet, Tri-Hexagon, and Concentric), all tested against PET. The voltage for each pattern was determined by averaging ten maximum peak-to-peak readings per sample. The data presented are the mean values from three independently fabricated and tested samples (n=3). Error bars represent the standard deviation. The tri-hexagon pattern produced a significantly higher voltage output (~11.3 V), more than double that of the lowest-performing Line pattern (~5.1 V). Figure 3. Optimization of triboelectric output through 3D printing infill patterns. (a) Schematic illustrations of the six distinct infill patterns tested for the thermoplastic polyurethane (TPU): (i) Line, (ii) Grid, (iii) Cubic, (iv) Octet, (v) Tri-Hexagon and (vi) Concentric. (b) A representative oscilloscope waveform of output voltage generated by the optimal tri-hexagon patterned TPU paired with a polyethylene terephthalate (PET). The signal corresponds to the highest recorded mean peak-to-peak voltage of approximately 11.3 V. (c) A graph comparing the mean peak-to-peak voltage output for TPU layers printed with the different infill patterns (Line, Grid, Cubic, Octet, Tri-Hexagon, and Concentric), all tested against PET. The voltage for each pattern was determined by averaging ten maximum peak-to-peak readings per sample. The data presented are the mean values from three independently fabricated and tested samples (n=3). Error bars represent the standard deviation. The tri-hexagon pattern produced a significantly higher voltage output (~11.3 V), more than double that of the lowest-performing Line pattern (~5.1 V).

Effect of layer height

After selecting the material and optimizing the infill pattern, we systematically varied the layer height of 3D-printed TPU to further enhance the triboelectric output. Layer height, representing the vertical thickness of each layer in the additive manufacturing process, directly affects the triboelectric properties of the printed structure (21). Starting from 0.2 mm up to 1.2 mm with 0.2 mm increment, our results identified 0.4 mm as the optimal layer height, achieving a peak voltage of 11 V (standard deviation of 0.51 V) at a tapping frequency of approximately 3 Hz and an applied force of 1.8 N **(Figure 4a)**. Performance was reduced at both lower and higher layer heights **(Figure 4b)**.

Application based performance of the optimized TENG

The practical applicability of the optimized TENG configuration—comprising a TPU/PET pair, a tri-hexagonal infill pattern, and a 0.4 mm layer height—was evaluated through a series of functional tests. First, the standalone performance was characterized. The optimized sample was shown to successfully charge a 2.2 μF capacitor to 1.6 V within approximately 50 seconds under random manual tapping **(Figure 5a)**. Furthermore, peak output voltages of up to 30 V were generated under similar tapping conditions demonstrating a high responsiveness to varying force magnitudes **(Figure 5b)**. Finally, the effective electricity generation capability was confirmed by illuminating 20 blue light-emitting diodes (LEDs) connected in series **(Figure 5c)**.

Subsequently, a scaled bridge model was fabricated to demonstrate the potential for structural integration. Three TENG units, operating on a hybrid sliding and contact-separation mode, were constructed. Each unit was encased within a compact, 3D-printed cylindrical enclosure. In this design, the tribo-negative PET layer was wrapped around a cylindrical slider, while the optimized tribo-positive TPU layer was affixed to the stationary inner lining of the casing **(Figure 5d)**. The three TENG cylinders were strategically positioned at the base of the bridge model **(Figure 6a)**. The electrical outputs of the three TENG units were connected in series to amplify the overall voltage. The performance of the integrated system was evaluated under three types of manually applied mechanical stress: pressing, shaking, and ball impact. Voltage

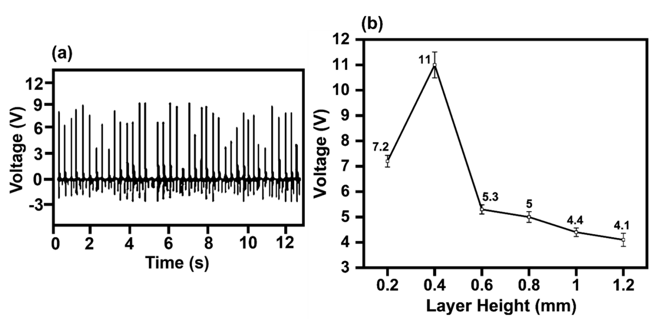

Figure 4. Optimization of triboelectric output through 3D printing layer height. (a) A representative oscilloscope waveform of the output voltage generated by the optimal 0.4 mm layer height configuration. The signal was produced by a tri-hexagon patterned thermoplastic polyurethane (TPU) and a polyethylene terephthalate (PET), demonstrating the highest mean peak-to-peak voltage of approximately 11 V. (b) A graph comparing the mean peak-to-peak voltage output for TPU layers printed with varying layer heights, ranging from 0.2 mm to 1.2 mm in 0.2 mm increments. All samples featured the optimized tri-hexagon infill pattern and were tested against a PET film. The voltage for each layer height was determined by averaging ten maximum peak-to-peak readings per sample. The data presented are the mean values from three independently fabricated and tested samples (n=3). Error bars represent the standard deviation. The 0.4 mm layer height yielded the maximum output, with a notable decrease in performance observed at both lower and higher layer heights.

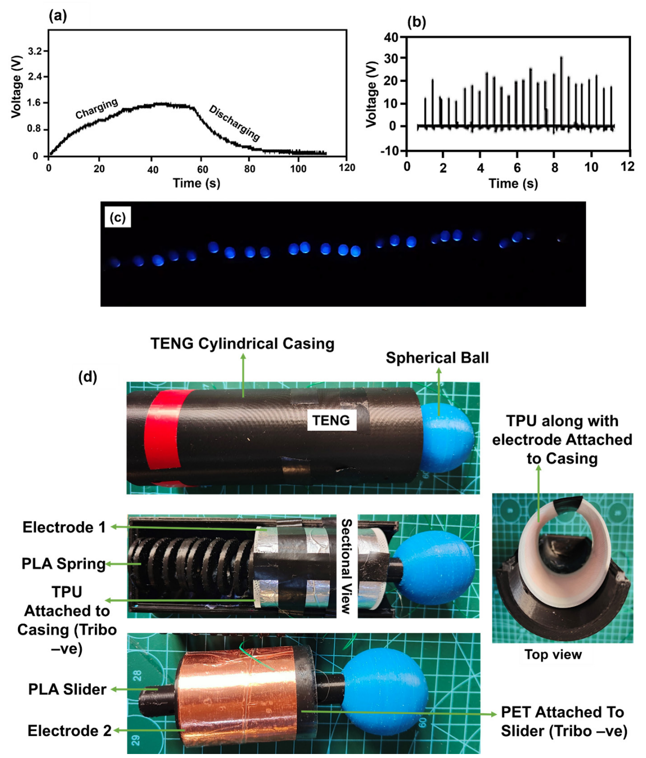

Figure 5. Application-based performance of the optimized triboelectric nanogenerator (TENG) and its structural components. (a) The charging and discharging cycle of a 2.2 μF capacitor, powered solely by the optimized TENG under random manual tapping. The capacitor charged to 1.6 V in approximately 50 seconds, demonstrating the device's energy storage capability. (b) A representative voltage output waveform showing a peak of 30 V generated by the optimized TENG. This signal was produced by applying manual, non-periodic impacts of varying force using a finger, simulating irregular environmental vibrations. (c) Photograph of 20 blue light-emitting diodes (LEDs) illuminated in series by the optimized TENG under tapping, confirming its ability to directly power low-power electronics. The TENG used for tests (a-c) had an active area of 3 cm x 3 cm and was composed of a tri-hexagon patterned thermoplastic polyurethane (TPU) layer (0.4 mm layer height) as the tribo-positive material and a polyethylene terephthalate (PET) as the tribo-negative material. (d) Exploded schematic and components of the cylindrical TENG unit designed for the bridge prototype. From top to bottom: the fully assembled cylindrical TENG; a sectional view showing the internal slider and the stationary casing; the polylactic acid (PLA) casing with the optimized TPU layer affixed to its inner lining; the 3D-printed PLA spring; the cylindrical slider with the PET layer wrapped around its circumference and a spherical ball on top for multi-directional actuation; and a top-down view of the casing showing the circular TPU lining. The device operated in a hybrid sliding/contact-separation mode to harvest energy from multi-directional bridge vibrations.

https://doi.org/10.59720/25-003

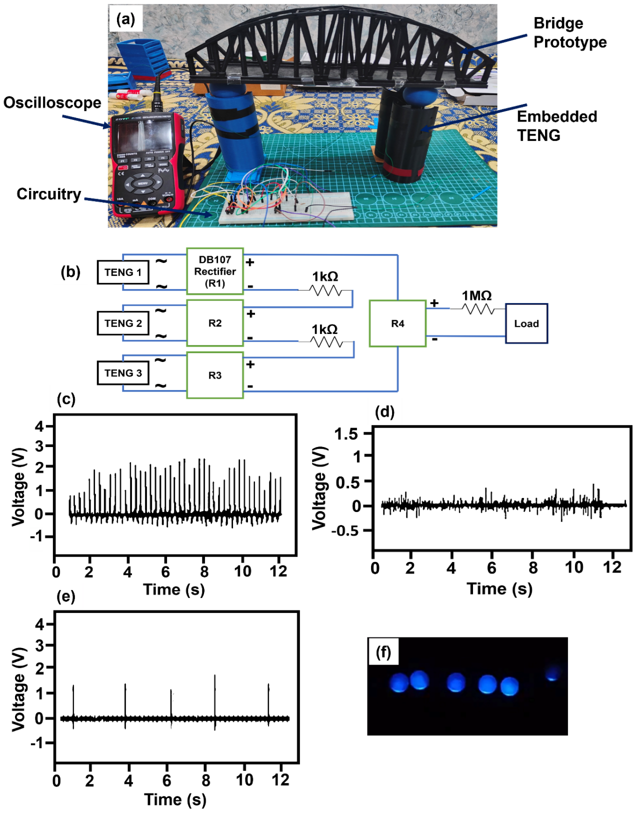

Figure 6. Performance of the 3D-printed bridge prototype integrated with triboelectric nanogenerators (TENGs). (a) Photograph of the scaled bridge model with three cylindrical TENG units mounted at its base. (b) The electrical schematic for the energy harvesting circuit, where the three TENGs are connected in series. Their combined alternating current (AC) output is rectified to direct current (DC) by a DB107 full-bridge rectifier module (R4) and their individual output is rectified by three other rectifiers of same model (R1, R2 and R3). The circuit includes two 1 kΩ resistors and 1 MΩ resistor for voltage regulation, with the output used to power a load of five light-emitting diodes (LEDs) in series. (c) Oscilloscope voltage waveform generated by manually pressing down on the bridge deck producing a peak voltage of approximately 3 V. (d) Voltage waveform generated by manually shaking the entire bridge model back-and-forth producing a peak voltage of approximately 0.5 V. (e) Voltage waveform generated by dropping a 20 g ball from a height of 10 cm onto the bridge deck (Impact force of 2.4 N), producing a peak voltage of approximately 2 V. (f) Photograph of five blue LEDs being illuminated by the electrical energy harvested from the pressing motion shown in (c). All voltage values are the result of the three series-connected TENGs operating simultaneously and represent the raw, unprocessed output from the bridge prototype.

waveforms recorded by an oscilloscope confirmed successful energy harvesting and conversion, with measurable voltages generated in each scenario. Approximate peak voltages of 3 V were observed during pressing, 0.5 V during shaking, and 2 V upon the impact of a dropped ball **(Figure 6c-e)**.

DISCUSSION

This study demonstrated the potential of 3D-printed triboelectric nanogenerators (TENGs) as sustainable energy solutions for structural health monitoring. We hypothesized that optimizing specific 3D printing parameters—namely the infill pattern and layer height—would enhance the energy output of TENGs by increasing the effective contact area for triboelectrification. Our data strongly support this hypothesis, revealing that material selection, structural design, and geometric parameters are critical for efficient energy conversion.

A key finding was the improved performance of the TPU/PET material pair, which produced a peak voltage output of ~11 V, far surpassing the ~0.66 V from TPU/ABS. This was attributed to the strong triboelectric polarity contrast between TPU and PET, that enhanced static charge generation and maximized energy conversion efficiency (19). This confirms its suitability as the most effective material pairing for our prototype.

Structural optimization through infill patterning proved highly impactful. The tri-hexagonal pattern generated ~11.3 V, nearly double the output of the line pattern (~5.1 V). This improved performance was a direct result of its unique geometric structure, which maximizes contact points and enhances frictional interaction. The combination of interlocking triangles and hexagons creates a high-density contact surface, facilitating more efficient charge transfer with each mechanical impact compared to simpler patterns like the linear arrangement (20).

Furthermore, layer height emerged as a crucial geometric factor, with 0.4 mm achieved the highest output. The optimal performance at this height stems from a critical balance between force sensitivity and effective surface interaction. At greater layer heights, the force required for triboelectric generation increases due to reduced surface contact, leading to suboptimal charge transfer. Conversely, layer heights below 0.4 mm can expose underlying electrodes through surface gaps, causing rapid charge dissipation (21). Thus, the 0.4 mm height minimizes energy losses while maximizing surface interaction, validating our design approach.

The practical relevance of these optimizations was confirmed through application-based testing. The optimized TENG successfully powered 20 LEDs, charged a capacitor, and generated high voltages under random tapping, demonstrating its potential for low-power electronics. Furthermore, when integrated into a scaled bridge model, the TENG system effectively harvested energy from various simulated vibrations, including pressing, shaking, and impacts. These results demonstrate the feasibility of the TENG prototype for harnessing vibrational energy. While the current output is insufficient for powering high-energy devices, the TENG effectively harvested energy from feeble vibrations. The TENG prototypes developed in this study demonstrate a viable pathway toward self-powered structural health monitoring. With further enhancements to overcome current limitations, devices based on these optimized 3D-printing principles could be used to develop TENGs that can be deployed on actual bridges to harvest ambient energy efficiently. This would contribute to sustainable infrastructure monitoring, aligning with the broader goal of powering low-power electronics from otherwise wasted mechanical energy.

This study had several limitations. The temperature and humidity were not precisely controlled, which are known to significantly influence triboelectric output. Further, the prototypes were fabricated on a small scale using

https://doi.org/10.59720/25-003

commercially available materials and tested under manual actuation, which introduces variability. Also, the specific values for material purity and surface roughness were not disclosed by the vendors and were not independently characterized in this study. Consequently, the sensitivity to detect very subtle vibrations and the overall energy output require further improvement for mass-level deployment. Finally, scalability to larger, industrially relevant dimensions remains a significant challenge. Future work will therefore focus on addressing these limitations by developing larger and more durable prototypes using industry-grade materials, conducting tests in controlled environmental chambers to quantify the impact of temperature and humidity, refining the TENG design to improve sensitivity for detecting subtle motions while maintaining robust energy harvesting capability and exploring product design and manufacturing strategies suitable for mass production. These steps are essential for assessing the practical viability of these devices for real-world applications.

In conclusion, this study demonstrates a systematic approach to optimizing 3D-printed TENGs by tuning material combinations and printing parameters, resulting in a peak voltage output of up to 11.3 V using TPU/PET, a tri-hexagonal infill pattern, and a 0.4 mm layer height. The optimized TENG successfully powered 20 LEDs, charged a 2.2 μF capacitor to 1.6 V, and was integrated into a scaled bridge prototype where it harvested voltages of approximately 3 V by pressing down on the bridge, 2 V by ball impact, and 0.5 V by shaking it. These results validate the device's effectiveness for low-power energy harvesting and sensing applications.

MATERIALS AND METHODS

Materials

All materials used in this study were commercially sourced from online platforms like Amazon (A), and Robu (R). The 3D printing filaments were all 1.75 mm in diameter. Thermoplastic Polyurethane (TPU) (R, eSUN eTPU-95A, SKU-1494066), used as the tribo-positive material, Acrylonitrile Butadiene Styrene (ABS) (R, eSUN ABS+, SKU-1552600) and Polylactic Acid (PLA) (R, eSUN PLA+, SKU-315610), used for TENG structural components (casing, slider, springs). All non-printed material surfaces were used as received from the supplier without additional treatment. Polyethylene Terephthalate (PET) (A, TrendMaker, B0FGQMDRF9), sheet with a thickness of ~0.12 mm, Copper Foil (A, ART IFACT, Cu0.1X50X1000), used for electrodes, thickness ~0.1 mm, Teflon (A, Hilitand, Hilitand4ihog7fsym), sheet with a thickness of ~0.1 mm and Kapton (Polyimide Tape) (A, Hxtape, Hx-JSZ), thickness 0.08 mm.

Triboelectric performance testing setup

A custom testing setup was designed to systematically measure the voltage output of different TENG configurations under consistent impact conditions **(Figure 1c)**. The setup consisted of a vertical testing tower with a tribo-positive "hitting medium" fixed at a consistent drop height of 2 cm using an adjustable fixture and a limiting clip. The tribo-negative material was mounted on a base plate connected to copper electrodes. A smooth, low-friction wire was attached to the hitting medium to manually lift and release it, allowing it to fall freely under gravity. The manual actuation was performed at an approximate frequency of 3 Hz. The output voltage was recorded in real-time using a Zoyi (ZT 703S, 0624RE0046) oscilloscope multimeter.

Experimental design and optimization protocol

The optimization process focused on three parameters: material pairing, infill pattern, and layer height. All samples were printed and tested at room temperature (24 °C). For each experimental condition, three independent samples were fabricated and tested. For material pairing the tribo-positive material was consistently TPU. The following tribo-negative materials were tested: ABS, kapton, copper, PLA, teflon, and PET. For infill pattern optimization six distinct infill patterns were evaluated for the TPU layer: line, concentric, grid, cubic, octet, and tri-hexagon **(Figure 3a)**. For layer height optimization, the layer height of the TPU structure was systematically varied from 0.2 mm to 1.2 mm in increments of 0.2 mm. For every sample, the voltage output was calculated by averaging ten maximum peak-to-peak readings from the oscilloscope. The final value for each condition was reported as the mean of the three independent trials, with the standard deviation used to quantify variability.

Fabrication of TENG components and bridge prototype

The TENG components were designed in SolidWorks and sliced using Creality Slicer software. All 3D printing was performed on a Creality Ender 3 printer using standard 3D printing parameters as per material guidelines provided by manufacturer **(Table 1)**. The cylindrical TENG casing (50 mm height × 15 mm diameter, 2 mm wall thickness) and the internal slider were printed using PLA filament. The casing was printed in two semi-cylindrical sections for easy assembly. The optimized TPU layer (0.4 mm height, tri-hexagonal infill) was affixed to the inner lining of the casing, and the PET layer was attached to the outer circumference of the slider using a standard hot-glue gun. Copper electrodes were attached to both layers. The slider was mounted on a 3D-printed PLA spring at the base of the casing to ensure it returned to its original position after actuation. For the bridge

Printing Parameter	TPU	PLA
Infill	100%	60%
Printing speed	40 mm/s	60 mm/s
Infill pattern	Line, concentric, grid, cubic, octet and tri-hexagon	Line
Nozzle temperature	230ºC	200ºC
Build plate temperature	70ºC	50ºC
Base layer height	0.15 mm	0.2 mm

Table 1. Standard 3D printing parameters for thermoplastic polyurethane (TPU) and polylactic acid (PLA) filaments. These parameters were selected based on manufacturer recommendations to ensure proper extrusion and layer adhesion. The infill density, printing speed, nozzle temperature, build plate temperature, and base layer height were kept constant for all prints of a given material. For the TPU, the infill pattern was systematically varied between prints as a key experimental parameter, testing the following: line, concentric, grid, cubic, octet, and tri-hexagon. The PLA components (structural parts) were printed exclusively with a line infill pattern.

prototype, three identical TENG units were fabricated as described above. They were strategically placed at the base of a scaled bridge model. The TENGs operated in a hybrid sliding/contact-separation mode, with a 0.5 mm side gap between the slider and the TPU layer.

Bridge prototype testing and electrical measurement

The performance of the bridge-integrated TENGs was evaluated under three types of mechanical stress, applied manually to introduce real-world variability. For pressing, the bridge deck was pressed down firmly and quickly by hand, and then released. For shaking experiment, the entire bridge model was shaken manually back-and-forth randomly. For ball impact experiment, a 30 g steel ball was dropped from a height of 2 cm onto the bridge deck, yielding an approximate force of 1.8 N. We estimated the impact force using standard kinematic and dynamic equations as:

$$v = \sqrt{2gh} \quad \text{........(Eqn. 1)}$$

where, ‘v’ is the velocity at impact (m/s), ‘g’ is the acceleration due to gravity (9.8 m/s²), and ‘h’ is the drop height (m). The impact force was then estimated using:

$$F = \frac{mv}{t} \quad \text{........(Eqn. 2)}$$

where, F is the applied force (N), m is the mass of the falling object (kg), ‘v’ is the velocity at impact (m/s), and ‘t’ is the contact time during impact (s). In our optimization experiments, the object had a mass of 30 g (0.03 kg) and was dropped from a height of 2 cm (0.02 m), yielding an approximate force of 1.8 N. For pressing and shaking, we calculated the reported voltage as the average of five maximum peak-to-peak values. For the ball-dropping test, we averaged all five recorded peaks to determine the final voltage value. The output voltage from the three TENGs connected in series was recorded using an oscilloscope.

For the capacitor charging and LED illumination tests **(Figure 5a-c, 6f)**, the AC output from the TENG was rectified to DC using a full-wave bridge rectifier composed of four DB107 diodes. Voltage regulation was achieved using a voltage divider network with two 1 kΩ resistors and one 1 MΩ resistor. The refined output was used to charge a 2.2 μF capacitor and to power five blue LEDs connected in series, with the entire circuit assembled on a breadboard.

ACKNOWLEDGMENTS

We would like to acknowledge Aashna Saraf, Founder of CreatED for providing valuable feedback and guidance throughout the project.

Received: January 06, 2025
Accepted: May 27, 2025
Published: July 19, 2026

REFERENCES

1. Wang, Zhong Lin, et al. “Progress in Nanogenerators for Portable Electronics.” *Materials Today*, vol. 15, no. 12, Dec. 2012, pp. 532–543. DOI: https://doi.org/10.1016/S1369-7021(13)70011-7.
2. Zi, Yunlong, et al. “Standards and Figure-of-Merits for Quantifying the Performance of Triboelectric Nanogenerators.” *Nature Communications*, vol. 6, no. 1, Sep. 2015, p. 8376. DOI: https://10.1038/ncomms9376.
3. Yang, Ya, et al. “A Single-Electrode Based Triboelectric Nanogenerator as Self-Powered Tracking System.” *Advanced Materials*, vol. 25, no. 45, Oct. 2013, pp. 6594–6601. DOI: https://doi.org/10.1002/adma.201302453.
4. Cui, Nuanyang, et al. “Dynamic Behavior of the Triboelectric Charges and Structural Optimization of the Friction Layer for a Triboelectric Nanogenerator.” *ACS Nano*, vol. 10, no. 6, April 2016, pp. 6131–6138. DOI: https://doi.org/10.1021/acsnano.6b02076.
5. Xu, Cheng, et al. “On the Electron-Transfer Mechanism in the Contact-Electrification Effect.” *Advanced Materials,* vol. 30, no. 15, March 2018, p. 1706790. DOI: https://doi.org/10.1002/adma.201706790.
6. Lowell, J., et al. “Contact Electrification: Why Is It Variable?” *Journal of Physics D: Applied Physics*, vol. 21, no. 1, 1988, pp. 125–132. DOI: https://10.1088/0022-3727/21/1/018.
7. Wang, Zhong Lin. “On the First Principle Theory of Nanogenerators from Maxwell's Equations.” *Nano Energy*, vol. 68, Feb. 2020, p. 104272. DOI: https://doi.org/10.1016/j.nanoen.2019.104272.
8. Wang, Sihong, et al. “Nanoscale Triboelectric-Effect-Enabled Energy Conversion for Sustainably Powering Portable Electronics.” *Nano Letters*, vol. 12, no. 12, Nov. 2012, pp. 6339–6346. DOI: https://doi.org/10.1021/nl303573d.
9. Niu, Simiao, et al. “A Universal Self-Charging System Driven by Random Biomechanical Energy for Sustainable Operation of Mobile Electronics.” *Nature Communications*, vol. 6, no. 1, Dec. 2015, p. 8975. DOI: https://doi.org/10.1038/ncomms9975.
10. Liu, Mengmeng, et al. “Large-Area All-Textile Pressure Sensors for Monitoring Human Motion and Physiological Signals.” *Advanced Materials*, vol. 29, no. 41, Sep. 2017, p. 1703700. DOI: https://doi.org/10.1002/adma.201703700.
11. Pang, Yaokun, et al. “Multilayered Cylindrical Triboelectric Nanogenerator to Harvest Kinetic Energy of Tree Branches for Monitoring Environment Condition and Forest Fire.” *Advanced Functional Materials*, vol. 30, no. 32, June 2020, p. 2003598. DOI: https://doi.org/10.1002/adfm.202003598.
12. Sun, Na, et al. “Waterproof, Breathable, and Washable Triboelectric Nanogenerator Based on Electrospun Nanofiber Films for Wearable Electronics.” *Nano Energy*, vol. 90, Dec. 2021, p. 106639. DOI: https://doi.org/10.1016/j.nanoen.2021.106639.
13. Delgado-Alvarado, Enrique, et al. “Recent Progress of Nanogenerators for Green Energy Harvesting: Performance, Applications, and Challenges.” *Nanomaterials,* vol. 12, no. 15, July 2022, p. 2549. DOI: https://doi.org/10.3390/nano12152549.
14. Niu, Simiao, et al. “Optimization of Triboelectric

Nanogenerator Charging Systems for Efficient Energy Harvesting and Storage." *IEEE Transactions on Electron Devices*, vol. 62, no. 2, Dec. 2014, pp. 641–647. DOI: https://doi.org/10.1109/TED.2014.2377728.
15. Zhu, Guang, et al. "Self-Powered, Ultrasensitive, Flexible Tactile Sensors Based on Contact Electrification." *Nano Letters*, vol. 14, no. 6, May 2014, pp. 3208–3213. DOI: https://doi.org/10.1021/nl5005652.
16. Agrawal, Kavya and Asrar Rafiq Bhat. "Advances in 3D printing with eco-friendly materials: a sustainable approach to manufacturing." *RSC Sustainability*, vol. 3, no. 6, May 2025, pp. 2582-2604. DOI: https://doi.org/10.1039/D4SU00718B.
17. Shahrubudin, Nurhalida, et al. "An overview on 3D printing technology: Technological, materials, and applications." *Procedia Manufacturing*, vol. 35, Aug. 2019, pp. 1286-1296. DOI: https://doi.org/10.1016/j.promfg.2019.06.089.
18. Shen, Rulin, et al. "High-Sensitivity and High-Resolution Triboelectric Acoustic Sensor for Mechanical Equipment Monitoring." *Nano Energy*, vol. 193, Jan. 2024, p. 110450. DOI: https://doi.org/10.1016/j.nanoen.2024.110450.
19. Hau, Ngoc Mai, et al. "Ultra-Stretchable and Shape-Memorable Ability of an Output-Boosted Triboelectric Nanogenerator Utilizing Highly Ordered Microdome-Crowning Thermoplastic Polyurethane for a Finger-Motion Detection Sensor." *Materials Advances*, vol. 4, no. 24, Nov. 2023, pp. 6568–6577. DOI: https://doi.org/10.1039/D3MA00534H.
20. Qiao, Haiyu, et al. "3D Printing Individualized Triboelectric Nanogenerator with Macro-Pattern." *Nano Energy,* vol. 50, Aug. 2018, pp. 126–132. DOI: https://doi.org/10.1016/j.nanoen.2018.04.071.
21. Chen, Chaojie, et al. "A Method for Quantitatively Separating the Piezoelectric Component from the As-Received 'Piezoelectric' Signal." *Nature Communications*, vol. 13, no. 1, March 2022, p. 1391. DOI: https://doi.org/10.1038/s41467-022-29087-w.